Viscoelastic Taylor-Couette Instability of Shear Banded Flow

Suzanne M. Fielding*

Department of Physics, University of Durham, Science Laboratories, South Road, Durham, DH1 3LE, United Kingdom

(Received 13 December 2009; revised manuscript received 24 February 2010; published 11 May 2010)

We study numerically shear banded flow in planar and curved Couette geometries. Our aim is to capture two recent observations in shear banding systems of roll cells stacked in the vorticity direction, associated with an undulation of the interface between the bands. Depending on the degree of cell curvature and on the material's constitutive properties, we find either (i) an instability of the interface between the bands driven by a jump in second normal stress across it or (ii) a bulk viscoelastic Taylor-Couette instability in the high shear band driven by a large first normal stress within it. Both lead to roll cells and interfacial undulations but with a different signature in each case, thereby suggesting that the roll cells in each of the recent experiments are different in origin.

DOI: 10.1103/PhysRevLett.104.198303 PACS numbers: 83.60.Bc, 47.20.Gv, 47.50.−d

The Taylor-Couette instability that arises when a Newtonian fluid is sheared between concentric cylinders has a long history in classical hydrodynamics, dating back to the ground breaking paper of Taylor in 1923 [1]. The effect is inertial in origin: fluid is forced centrifugally outward along the radial direction r, and recirculates via roll cells stacked in the vorticity direction z. For non-Newtonian complex fluids, the past two decades have seen considerable interest in an inertialess, *viscoelastic* Taylor-Couette (VTC) instability [2] that originates instead in the hoop stresses (first normal stresses) that arise when a polymeric fluid is sheared in a curved geometry. These squeeze fluid radially inwards, again triggering an instability that leads to roll cells stacked along z.

Another intensely studied flow phenomenon in complex fluids is that of "shear banding" [3], in which an initially homogeneous shear flow gives way to a state of coexisting bands of unequal viscosities and internal structuring, with layer normals in the flow-gradient direction r. Close analogies exist between this nonequilibrium transition and conventional equilibrium phase coexistence. There are also fundamental differences, e.g., in the way the coexistence state is selected in the absence of a free energy minimization principle [4]. Beyond the basic observation of banding, an accumulating body of data shows that many (perhaps most) shear banded flows show complicated spatiotemporal patterns and dynamics [5]. These are often associated with vorticity bands and/or roll cells stacked along z, in both curved Couette [6,7] and planar [8] flow geometries, the origin of which is unclear.

In this Letter, we give the first theoretical evidence to suggest that, in a curved flow, these rolls can arise via a mechanism in which the high shear band, once formed, develops a large enough first normal stress N_{1h} to trigger a further bulk instability of the VTC type within itself. We further show that this bulk instability disappears below a critical value of the cell curvature q, depending in a quantifiable way on the fluid's constitutive properties, consistent with the known scaling variable $\dot{\gamma}q^{1/2}$ for VTC (in)stability [2]. At small curvatures, however, a different instability emerges, originating at the interface *between* the bands. This instability was originally reported in planar flow in Ref. [9]. Important additional contributions here are to show it to be (i) controlled by the jump ΔN_2 in *second* normal stress across the interface and (ii) suppressed by curvature. It also leads to roll cells, but with identifiably different properties from those of the bulk instability. By mapping a full phase diagram of the two separate instabilities, we suggest that the different experimental observations of roll cells [6,8] have different origins.

Our study therefore brings together three different hydrodynamic instabilities in complex fluids: shear banding itself, instability of an interface between bands, and, for the first time theoretically, a bulk VTC-like instability of one band. We hope thereby to stimulate further experiments, in a family of flow cells of different curvatures, to verify (or otherwise) our findings with regards to this strikingly rich array of hydrodynamic instabilities.

We assume inertialess Stokes flow in which the total deviatoric stress tensor $\boldsymbol{T}$ obeys

$$0 = \nabla \cdot (\boldsymbol{T} - P\boldsymbol{I}) = \nabla \cdot (\boldsymbol{\Sigma} + 2\eta \boldsymbol{D} - P\boldsymbol{I}). \quad (1)$$

We have further assumed $\boldsymbol{T}$ to comprise two contributions: the term $2\eta\boldsymbol{D}$ is due to the Newtonian solvent, with η the solvent viscosity and $\boldsymbol{D}$ the symmetric part of the velocity gradient tensor, $(\nabla \boldsymbol{v})_{\alpha\beta} \equiv \partial_\alpha v_\beta$. The term $\boldsymbol{\Sigma}$ is the stress of the viscoelastic component, assumed to obey diffusive Johnson-Segalman dynamics [10]

$$\tau(\partial_t + \boldsymbol{v} \cdot \nabla)\boldsymbol{\Sigma} = a\tau(\boldsymbol{D} \cdot \boldsymbol{\Sigma} + \boldsymbol{\Sigma} \cdot \boldsymbol{D}) + \tau(\boldsymbol{\Sigma} \cdot \boldsymbol{\Omega} - \boldsymbol{\Omega} \cdot \boldsymbol{\Sigma}) + 2\eta_p \boldsymbol{D} - \boldsymbol{\Sigma} + \ell^2 \nabla^2 \boldsymbol{\Sigma}. \quad (2)$$

Here η_p is the viscoelastic contribution to the (zero) shear viscosity, τ the viscoelastic relaxation time, and $\boldsymbol{\Omega}$ the antisymmetric part of $\partial_\alpha v_\beta$. The slip parameter a, which obeys $-1 \leq a \leq 1$, measures the nonaffinity (fractional stretch) of polymeric deformation compared to the flow. For $|a| < 1$ (slip) the underlying constitutive curve can be nonmonotonic, triggering shear banding. The diffusive

term $\nabla^2\boldsymbol{\Sigma}$ is physically relevant [11] whenever stress heterogeneities occur on microscopic scales. For shear banded flows it ensures unique selection of the shear stress at which banding occurs [4], and its prefactor sets the thickness $O(\ell)$ of the interface between the bands.

We study flow between concentric cylinders of radii R_1, R_2, in cylindrical coordinates r, θ, z. The inner cylinder rotates at speed V; the outer is fixed. We denote the cell curvature by $q = (R_2 - R_1)/R_1$. The flat limit of planar Couette flow corresponds to $R_1 \to \infty$ at fixed $R_2 - R_1$, and so $q \to 0$. (At $q = 0$ we use x, y, z to denote flow, flow gradient, and vorticity directions. The first and second normal stresses are then $N_1 = \Sigma_{xx} - \Sigma_{yy}$, $N_2 = \Sigma_{yy} - \Sigma_{zz}$.) The natural bulk rheological variables are the cylinder velocity V, which is the main experimental control parameter, and the torque $\tilde{\Gamma} = q^2\Gamma$ (with $\tilde{\Gamma} \to T_{xy}$ as $q \to 0$). We assume invariance with respect to θ and study dynamics in the flow-gradient and vorticity plane rz, the most commonly imaged experimentally. At the cylinders we assume boundary conditions [12] of zero flux normal to the wall $\hat{\hat{n}} \cdot \nabla\Sigma_{\alpha\beta} = 0 \ \forall \ \alpha, \beta$ for the viscoelastic stress; and no slip or permeation for the velocity. The height of the simulated region in the vorticity direction is L_z, with periodic boundaries.

We use units of length in which the rheometer gap $R_2 - R_1 = 1$, of time in which the viscoelastic relaxation time scale $\tau = 1$, and of mass in which the polymer viscosity obeys $\eta_p = 1$. This leaves parameters a, q, η, l, L_z. All results below have (i) $\eta = 0.05$, a typical experimental viscosity of the high shear band [6,8], (ii) estimated interfacial width $\ell \approx (k_B T/G)^{1/3} \approx 0.0025$ [11] using linear rheology [6] for the shear modulus G, but see Ref. [8] for a current debate, and (iii) cell height $L_z = 2.0$, the maximum feasible numerically. Parameter sensitivity is briefly as follows. (i) Halving the solvent viscosity η shifts both stability boundaries in Fig. 3 (bottom) more unstable by about $1/4$ decade. (ii) Doubling the interfacial width ℓ has no effect (to within the accuracy of Fig. 3) on the bulk instability, as expected, but, also as expected [9], dramatically stabilizes the interfacial stability boundary by more than a decade. (iii) Increasing L_z to 3.0 has only a small effect on either boundary, showing finite size effects to be under control.

In our numerics, we change variables from (r, z) to (p, z) where $p = \ln(r/R_1)/\ln(R_2/R_1)$, thereby mapping our curved geometry onto an effectively flat one simulated on a regular rectangular grid (p_j, z_i) [10]. Components of the discretized governing equations are then evolved in time as for the flat limit [9]. Our code reproduces known results for (i) the instability of an interface between shear bands in planar flow [9], (ii) 1D banded states in curved Couette flow [10], (iii) dispersion relations and stability curves for VTC instability in the Oldroyd B model [2]. Our results have (convergence checked) time step and grids $(\Delta t, \Delta p, \Delta z) = (0.0002, \alpha/512, 1/512)$ with $\alpha = 1$ $(1/2)$ for unbanded (banded) base states.

First we discuss the results of 1D calculations that artificially assume translational invariance in z, allowing structure only in the main banding direction r. In the flat limit $q \to 0$, force balance dictates that the shear stress T_{xy} is uniform across the gap. Within the assumption of a similarly homogeneous shear rate, the constitutive relation is given by $T_{xy}(\dot{\gamma}) = \Sigma_{xy}(\dot{\gamma}) + \eta\dot{\gamma}$ where $\Sigma_{xy}(\dot{\gamma})$ follows from solving Eq. (2) subject to invariance in time and space (thin solid line in Fig. 1, left; formula in Ref. [10]). For an applied shear rate in the region of negative slope, homogeneous flow is unstable and the system separates into coexisting bands at a selected stress $T_{\rm sel}\sqrt{1-a^2} = 0.483$. The steady state bulk flow curve thus shows a plateau in the banding regime (thick solid line in Fig. 1, left), at this single value of the stress for which a stationary interface can exist between bands. For nonzero cell curvature the stress "plateau" acquires a slope [10]; see Fig. 1, right.

In what follows, we will exploit the fact that for all values of a in the allowed range $-1 \le a \le 1$ these 1D states collapse onto a single master state [10] in terms of the scaling variables $\dot{\gamma}\sqrt{1-a^2}$, $V\sqrt{1-a^2}$, $\Gamma\sqrt{1-a^2}$, $\Sigma_{xy}\sqrt{1-a^2}$, $\Sigma_{xx}(1-a)$, and $\Sigma_{yy}(1+a)$, as used in Fig. 1. In particular, the first normal stress in the high shear band obeys $N_{1h} \sim 1/(1-a)$ as $a \to 1$. We therefore anticipate, and demonstrate below, that in curved cells there will arise a bulk instability of the VTC kind in this band for large $1/(1-a)$. Likewise the jump in second normal stress across the interface obeys $\Delta N_2 \sim 1/(1+a)$, and we show below that the instability of the interface between the bands is controlled by this variable. Note that we are using a as a parameter that *de facto* controls the relative strengths of these normal stresses N_{1h}, ΔN_2, and so (we show) of the two instabilities. In reality, these stresses are set by a combination of material properties such as micellar length and degree of branching.

We now turn to 2D simulations in the (r, z) plane. Each run has as its initial condition a 1D "basic state" as just

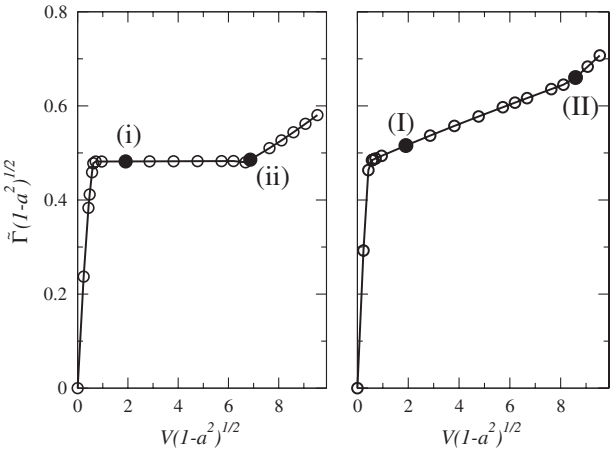

FIG. 1. Bulk flow curve of 1D base states for $q = 0.0$ (left), $q = 0.16$ (right). Symbols (i, ii, I, II) for reference in Figs. 2 and 3.

discussed, plus a tiny 2D perturbation. The early time evolution of the modes $\exp(ikz)\exp(\omega t)$ of this perturbation gives the dispersion relation $\omega(k)$, in which a maximum value $\omega^* > 0$ shows the basic state to be linearly unstable.

We start with a basic state comprising unbanded flow on the high shear branch. In a flat geometry this is linearly stable; solid line in Fig. 2, left. In contrast, in a curved device it becomes linearly unstable when the first normal stress exceeds a critical value, consistent with the onset of a bulk VTC-like instability; dashed line in Fig. 2, left. The presence of this instability in a flow state that resides fully on the high shear branch leads us to expect, in curved flow, a bulk instability of the VTC kind in the high shear band of a banded flow. Accordingly, we now turn to the stability properties of a banded basic state. We start with the flat case $q = 0$ before turning to the curved case $q > 0$.

Shear banded flow in a flat geometry $q = 0$ is already known [9] to show an instability of the interface between the bands, leading to undulations along the interface with wave vector $q_z \approx 2\pi/L_z$. In Ref. [9] we suggested this to be driven by a jump in normal stress across the interface, but did not study this in detail. By exploiting in this work the scaling of the normal stresses with a, we find convincing evidence that it is indeed driven by the jump ΔN_2 in second normal stress; Fig. 2, right.

So far we have brought together for the first time in the same model three instabilities already documented separately in the literature: shear banding itself [3], a VTC-like instability of a strongly sheared polymeric material with a large first normal stress in a curved geometry [2], and the instability in a flat geometry of an interface between shear bands with respect to undulations with wave vector in the vorticity direction [9], driven by the jump in second normal stress across the interface. Our most significant result, however, is to report the stability properties of a shear banded state in two situations not previously studied theoretically—in a curved flow cell, and when the high shear band has large first normal stress—thereby demonstrating a bulk VTC-like instability of the high shear band.

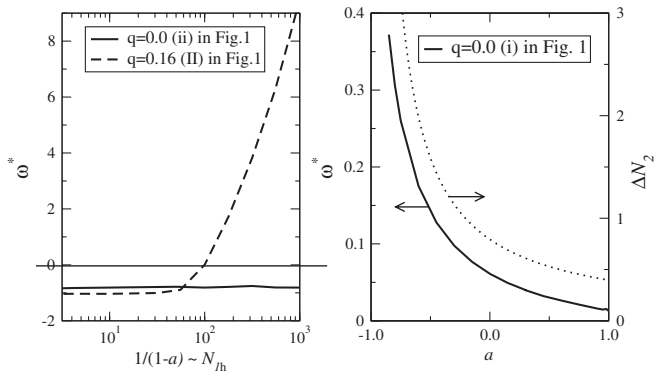

FIG. 2. Left: Maximum growth rate for an unbanded base state just into the high shear branch versus the first normal stress scaling variable $1/(1-a)$ for flat and curved cells: $(q, \dot{\gamma}(1-a^2)^{1/2}) = (0.0, 6.87), (0.16, 8.58)$. Bulk VTC instability is seen in the curved case at high N_{1h}. Right: Same for an applied shear rate $\dot{\gamma}(1-a^2)^{1/2} = 1.91$ in the banding regime in a flat geometry, showing interfacial instability. Also shown is the jump in second normal stress (dotted line).

As shown in Fig. 3, curvature suppresses the interfacial instability just discussed, dragging the weakly positive mode for $q = 0$ below the axis $\omega^* = 0$ (top two panels). For large enough curvature q or first normal stress $N_{1h} \sim 1/(1-a)$ in the high shear band, though, we find a crossover (interchange of dispersion maxima) to a different instability: now of the bulk VTC kind in the high shear band. At the interchange, the wavelength of the fastest growing mode switches (inset of Fig. 3, top right) from $\lambda \approx 1$, consistent with interfacial instability [9], to $\lambda \approx 1/8$, consistent [2] with a VTC instability in a bulk flow phase of width ≈ 0.3, for this applied shear rate. In Fig. 3 (bottom) we map out an entire phase diagram in the plane of curvature q versus first normal stress scaling variable $N_{1h} \sim 1/(1-a)$. The boundary of the VTC instability is seen to scale as $q \sim (1-a) \sim N_1^{-1} \sim \dot{\gamma}^{-2}$, consistent with the known criterion for the same instability in unbanded flow [2]. The same scaling is also seen for the boundary of the interfacial instability.

Gray-scale snapshots on the ultimate attractor for each kind of instability are shown in Fig. 4. The stress signals of

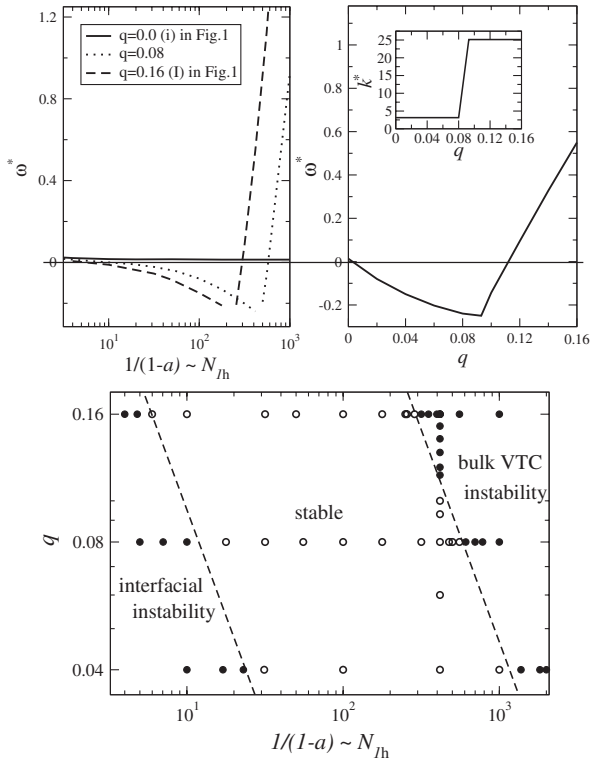

FIG. 3. Top left: Maximum growth rate for an applied shear rate $\dot{\gamma}(1-a^2)^{1/2} = 1.91$ in the banding regime versus the first normal stress scaling variable $N_{1h} \sim 1/(1-a)$ for three different cell curvatures q. Top right: Same versus cell curvature at fixed $1/(1-a) = 416$. Inset shows the wave vector. Bottom: Corresponding phase diagram in the plane of curvature versus first normal stress scaling variable. Dashed lines: Power -1.

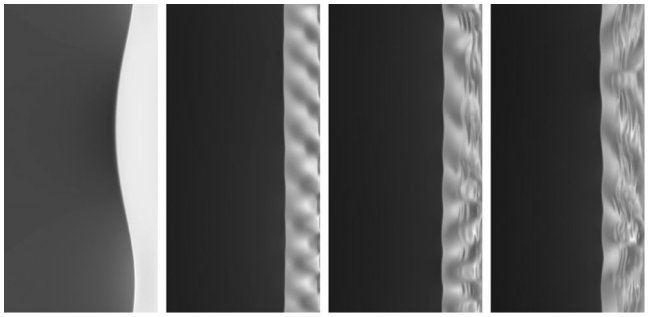

FIG. 4. Gray-scale snapshots of Σ_{xx} on the ultimate attractor in the p-z (horizontal-vertical) plane for a shear rate in the banding regime $\dot{\gamma}\sqrt{1-a^2} = 1.91$. Left: Interfacial instability in a flat cell $q = 0$ with $1/(1-a) = 1.43$. Others left to right: Bulk instability of the VTC kind in the high shear band for a large value of the first normal stress scaling variable $1/(1-a) = 416$, for curvatures $q = 0.115, 0.13, 0.16$.

the rightmost ones appear chaotic, consistent with the observation of complex roll cell dynamics in Ref. [6].

In conclusion, for large first normal stresses and cell curvature we have demonstrated a bulk instability of the VTC kind in a high shear band. For small curvatures we find an undulatory instability of the interface between the bands, as in Ref. [9] for $q = 0$. An important additional contribution has been to show this interfacial instability to be (i) driven by the jump in second normal stress across the interface and (ii) suppressed by curvature.

The diffusive Johnson-Segalman model is highly phenomenological, taking no explicit account of underlying molecular mechanisms (reptation, reaction, etc.). It further assumes a Newtonian high shear branch, contrary to experiment [8] (although instability prevents most studies reaching this branch). It should not, therefore, be seen as microscopically faithful to any given fluid, but rather as a minimal approach to capturing shear banding, and (crucially) to allowing the strength of the normal stress components in the bands to be tuned, giving insight to the mechanisms that drive the two separate instabilities.

Experimental data for normal stresses $N_1(\dot{\gamma})$, $N_2(\dot{\gamma})$ are rare in micelles, making it difficult to estimate N_{1h} in our Fig. 3 (bottom), although the data of Ref. [13] suggest $N_{1h} = O(10^3)$. We hope that this Letter will help stimulate further measurements of this quantity.

The main aim of this Letter has been to capture and rationalize two different experimental observations of roll cells in shear banded flows [6,8]. Nghe *et al.* [8] demonstrated an instability leading to rolls stacked along the vorticity direction z in a rectilinear microchannel. The lack of cell curvature suggests these experiments to correspond to (the pressure driven equivalent of [14]) our calculations for $q = 0$ in Fig. 3 (bottom), and so to a linear interfacial instability. Indeed, it has long been known that flows with parallel streamlines are linearly stable with respect to *bulk* perturbations, although a nonlinear (subcritical) instability cannot be ruled out [15].

Lerouge *et al.* [6] demonstrated roll cells stacked along z in a Couette cell of curvature $q \approx 0.08$, and estimated their high shear band to satisfy the criterion for bulk VTC instability, which would correspond to the top right of Fig. 3 (bottom). Indeed, the complex dynamics of Ref. [6] suggest VTC, although the smallest observed wavelength ≈ 0.5–1 might perhaps also be consistent with interfacial instability. To resolve this, it would be interesting to perform a series of experiments vertically scanning Fig. 3 (bottom) with a family of flow cells of different curvatures ($q \approx 0.05$–0.5 for Couette, $q = 0$ in planar flow). While the stability gap in Fig. 3 apparently covers an impractical range of q, smaller values of the viscosity η (not uncommon experimentally but difficult to access numerically) do narrow this, as noted above, such that it might indeed be spanned by a family of cells.

Other open questions include the interaction of these roll cells with unstable modes of wave vector in the flow direction [16] and the effect of stick-slip dynamics at the wall on this rich array of hydrodynamic phenomena.

S. F. thanks Mike Cates, Ron Larson, and Peter Olmsted for discussions, and EPSRC EP/E5336X/1 for funding.

*suzanne.fielding@durham.ac.uk

[1] G. Taylor, Phil. Trans. R. Soc. A **223**, 289 (1923).
[2] R. G. Larson, E. S. G. Shaqfeh, and S. J. Muller, J. Fluid Mech. **218**, 573 (1990); E. S. G. Shaqfeh, S. J. Muller, and R. G. Larson, *ibid.* **235**, 285 (1992).
[3] S. Manneville, Rheol. Acta **47**, 301 (2008); P. D. Olmsted, *ibid.* **47**, 283 (2008).
[4] C. Y. D. Lu, P. D. Olmsted, and R. C. Ball, Phys. Rev. Lett. **84**, 642 (2000).
[5] S. Fielding, Soft Matter **3**, 1262 (2007); S. Lerouge and J.-F. Berret, arXiv:0910.1854 [Adv. Polym. Sci. (to be published)].
[6] M. A. Fardin *et al.*, Phys. Rev. Lett. **103**, 028302 (2009); S. Lerouge, M. Argentina, and J. P. Decruppe, *ibid.* **96**, 088301 (2006); S. Lerouge *et al.*, Soft Matter **4**, 1808 (2008).
[7] L. Bécu *et al.*, Phys. Rev. E **76**, 011503 (2007); K. Kang *et al.*, *ibid.* **74**, 026307 (2006); V. Herle *et al.*, Phys. Rev. Lett. **99**, 158302 (2007).
[8] P. Nghe *et al.* (to be published).
[9] S. Fielding, Phys. Rev. E **76**, 016311 (2007).
[10] M. W. Johnson and D. Segalman, J. Non-Newtonian Fluid Mech. **2**, 255 (1977); P. D. Olmsted, O. Radulescu, and C. Y. D. Lu, J. Rheol. **44**, 257 (2000).
[11] S. M. Fielding and P. D. Olmsted, Eur. Phys. J. E **11**, 65 (2003).
[12] J. Adams, S. Fielding, and P. D. Olmsted, J. Non-Newtonian Fluid Mech. **151**, 101 (2008); L. Cook and L. Rossi, *ibid.* **116**, 347 (2004).
[13] H. Rehage and H. Hoffmann, Mol. Phys. **74**, 933 (1991).
[14] S. M. Fielding and H. J. Wilson, J. Non-Newtonian Fluid Mech. **165**, 196 (2010).
[15] A. N. Morozov and W. van Saarloos, Phys. Rev. Lett. **95**, 024501 (2005).
[16] S. M. Fielding, Phys. Rev. Lett. **95**, 134501 (2005).